Colloquium: Optical simulations of electron diffraction by carbon nanotubes*

A. A. Lucas, F. Moreau, and Ph. Lambin

Laboratoire de physique du solide, Facultés Universitaires Notre-Dame de la Paix, 61 rue de Bruxelles, B5000 Namur, Belgium

(Published 16 January 2002)

This colloquium discusses the atomic structure of carbon nanotubes as deduced from high-resolution electron microscopy and electron diffraction in transmission through a single nanotube. The principal features of the observed micrographs are interpreted in terms of the cylindrical, chiral geometry of the atomic distribution of single-wall or multiwall nanotubes. In order to better understand the mechanism of image formation in electron diffraction, the authors propose optical simulation experiments using a laser pointer and a little "diffraction laboratory on a slide." The simulations visibly reproduce all the features of the observed electron micrographs, namely, the quasihexagonal patterns of Bragg spots, the streaked nature of the spots, the doubling of the spot number induced by chirality, etc. The present colloquium should allow a general readership to appreciate the continuing efficiency and power of diffraction methods for the determination of the structure of macromolecules.

CONTENTS

I. INTRODUCTION

In the Periodic Table of the Elements carbon is listed as crystallizing in the hexagonal structure. This structure, illustrated in Fig. 1(a), consists of planar layers of carbon atoms arranged in honeycomb lattices called graphene sheets. Within a sheet, three of the four valence electrons of a carbon atom form three strong trigonal bonds to three equidistant neighbors 0.14 nm away. The fourth valence electrons from different carbon atoms interact to form weak π bonds perpendicular to successive sheets which are loosely piled up on top of each other every 0.34 nm in an alternating $ABAB\ldots$ sequence producing a three-dimensional hexagonal unit cell. There are various other stacking arrangements possible, but this need not concern us here. This allotrope, known as graphite, is the most stable and most abundant solid form of pure carbon found in nature. A slightly less stable and vastly less abundant crystallographic form is diamond, which has the cubic structure shown in Fig. 1(b). Here each atom is covalently bound to four neighbors at the apexes of a regular tetrahedron.

Until about 15 years ago such were the only known crystalline forms of solid carbon. Then in 1985, the science of carbon was unexpectedly enlarged by the discovery of an entirely new class of structures called *fullerenes* (Kroto *et al.*, 1985). The fullerenes first discovered are spheroidal molecules such as shown in Fig. 2 (Curl *et al.*, 1991). These molecular clusters are sometimes called "curved graphite" because of their obvious appearance as curved sheets of graphene, with the typical threefold coordination of each atom in a honeycomb lattice. Note, however, the presence, in the hexagonal network, of occasional pentagonal rings which cause the curvature and eventual closure of the graphene sheets (Curl *et al.*, 1991). Fullerene molecules are in turn able to crystallize in a variety of three-dimensional (3D) structures (Krätschmer *et al.*, 1990).

Fullerenes were discovered serendipitously in the soot formed when a hot carbon vapor (several thousand degrees) cools off and condenses into clusters in an inert gas atmosphere. The most abundant and most cel-

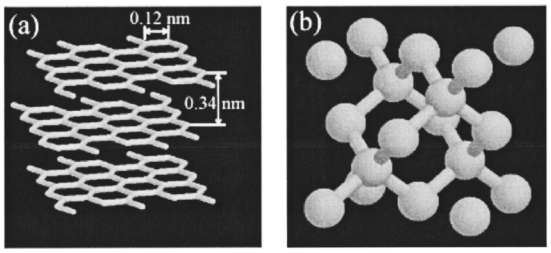

FIG. 1. The two traditional forms of crystalline carbon: (a) crystal structure of hexagonal graphite; (b) crystal structure of cubic diamond.

*This colloquium is adapted from the authors' chapter in *Nanostructured Carbon for Advanced Applications*, edited by G. Benedek, P. Milani, and V. G. Ralchenko (NATO Science Series, Vol. 24, Kluwer, Dordrecht, 2001).

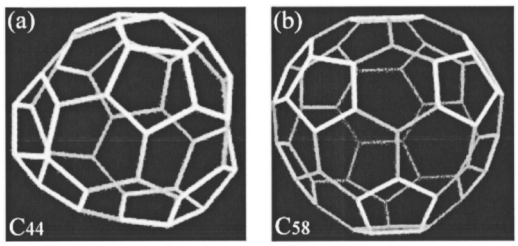

FIG. 2. Molecular structure of various globular fullerenes.

ebrated such molecule, C_{60} shown in Fig. 3(a), comprises 60 carbon atoms, all equivalent, regularly arranged in 12 pentagonal and 20 hexagonal rings, in a soccer ball arrangement. The 1996 Nobel prize in Chemistry was awarded to R. Curl, H. Kroto, and R. Smalley, the discoverers of this most beautiful molecule.

Five years after the initial discoveries, in 1990, a method was found to produce C_{60} and other fullerenes in large amounts. By simply striking an electric arc between two carbon electrodes (Krätschmer *et al.*, 1990), a soot is profusely generated which contains fullerenes in large proportion. Straightforward purification techniques of the soot soon made the pure fullerene materials available for fundamental studies. Thus it was found that, at room temperature, pure C_{60} crystallizes in a stable compact structure, usually the face-centered-cubic structure, an entirely new form of solid carbon called Fullerite (Huffman, 1991).

Beyond C_{60}, the next most abundant fullerene observed in the condensed carbon vapor is C_{70}, Fig. 3(b). This molecule can be conceived as being constructed by addition of a ring of ten atoms at one of the fivefold equators of C_{60}, as shown in Fig. 3(b). By adding successively n such parallel rings, while maintaining the graphitic threefold coordination, one can theoretically produce a series of cigar-shaped molecules C_{60+10n} [Figs. 3(c) and (d)]. In the limit of large n, these are particular members of a subfamily of fullerenes called *single-wall nanotubes*. In general, single-wall nanotubes can be conceived as any such long strip of graphene rolled up into a seamless cylinder. The latter can be left open or can be capped by hemifullerenes.

And indeed, in 1991, giant molecules with this topology were discovered in the carbon arc products (Iijima, 1991). However at first they were not observed as isolated species but only as part of *multiwall nanotubes*: these structures turn out to have a tree-ring organization of several coaxial single-wall nanotubes separated by the graphitic distance of 0.34 nm. This was first demonstrated by Iijima (1991) using high-resolution electron microscopy and electron diffraction. Soon afterwards suitable experimental conditions were found (Ebbesen *et al.*, 1992) to obtain abundant quantities of isolated single-wall nanotubes in the soot, again making this new material largely available for fundamental investigations (Ebbesen, 1994).

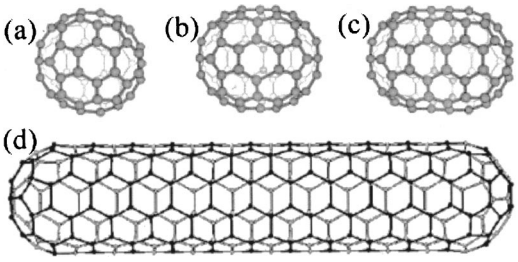

FIG. 3. From the globular to the tubular structure: (a) soccer ball structure of fullerene C_{60}; (b) rugby ball structure of fullerene C_{70}; (c) C_{80}; (d) tubular structure of C_{260}.

In the last few years, the pace of research on nanotubes has been accelerated by the discovery of the extraordinary electrical transport properties of single-wall nanotubes. Their conductivity is very sensitive to the detailed atomic structure of the nanotube, particularly its diameter (Dekker, 1999) and its so-called chiral or wrapping angle (see below): a slight change of the latter can result in the nanotube being either metallic or semiconducting. Such behavior, quite exceptional for a single element, could eventually bring about the birth of the much talked about molecular nanoelectronics (Dekker, 1999). Details on the methods of synthesis and on the potential applications of nanotubes can be found in recent reviews (Tanaka *et al.*, 1999; Zhen *et al.*, 1999).

As for practically all other large molecules, the atomic arrangement of nanotubes has been determined by diffraction methods. The present paper will attempt to describe the atomic structure of nanotubes such as revealed by electron microscopy and electron diffraction. First we explain qualitatively the formation of the images and diffraction patterns and then we present demonstration experiments which simulate the diffraction phenomenon optically. By using specially designed planar diffraction masks and a visible laser such as a laser pointer, we are able to reproduce, in the visible range, the essential features of the observed electron-diffraction patterns.

II. ELECTRON MICROSCOPY AND DIFFRACTION MICROGRAPHS OF NANOTUBES

A. Straight nanotubes

We begin by presenting selected electron microscopy and electron diffraction micrographs of nanotubes and we explain in simple terms the major characteristic features arising from their assumed underlying atomic structures.

Figure 4 sketches a typical electron-scattering experiment with an electron beam incident perpendicularly to a nanotube (Iijima, 1994). The disposition of the post-specimen electron optics determines whether the detector registers a high-resolution image of the specimen itself, Fig. 5(a), or a greatly enlarged image of the diffraction pattern produced by the specimen, Fig. 5(b). Such is the power of electron microscopy that the beam can be focused onto a selected area of the sample containing one single nanotube in the illuminated field of view. The vertical lines in Fig. 5(a) are shadow projec-

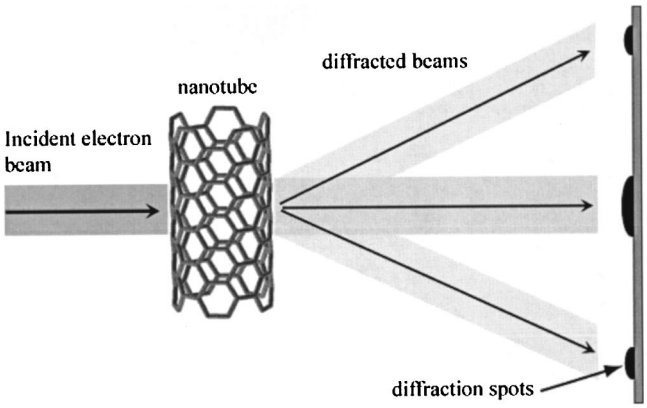

FIG. 4. Schematic representation of an electron-scattering experiment. The diffraction angles are grossly exaggerated. The size of the diffraction pattern needs to be enhanced by post-specimen magnifying optics (not represented).

tions of the nearly flat side walls of the nanotube: the electrons falling between the parallel quasiplanar sheets of carbon honeycomb lattice on either side of the nanotube are guided nearly freely through, while those falling onto the sheets tend to be deflected or blocked. The outer and inner diameters of the nanotube are 6 and 4.64 nm, respectively. This information is immediately revealed by the micrograph itself since the layers are assumed to be separated by the graphitic distance of 0.34 nm, which provides a metric to the picture (this assumption is of course consistent with the known calibrated magnification of the microscope). In effect, Fig. 5(a) represents a planar projection of the atomic density onto a plane perpendicular to the beam direction. However, the resolution (about 0.2 nm) of the microscope is not quite sufficient to resolve the individual atoms themselves separated only by 0.14 nm.

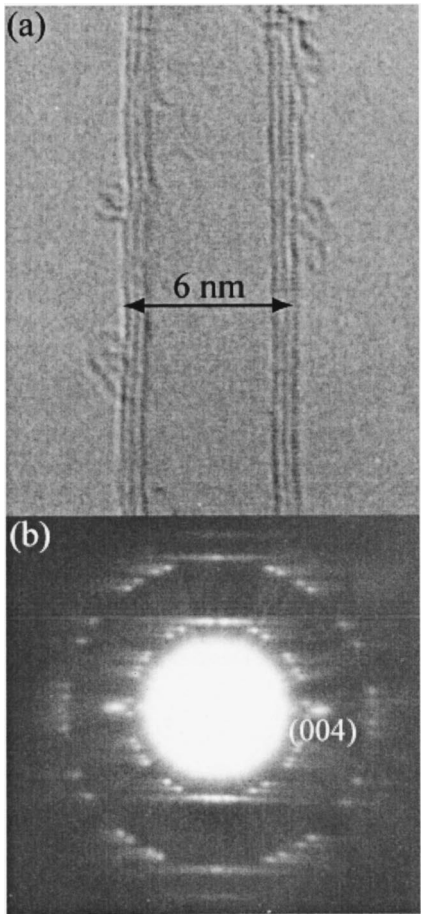

FIG. 5. The electron microscope imaging of a nanotube: (a) electron microscopy image of a triple layer nanotube (from Iijima, 1994); (b) electron-diffraction pattern of the nanotube in (a) at normal incidence.

The diffraction pattern of this triple-layer nanotube is presented in Fig. 5(b). Around the bright unscattered beam at the center, there are two circular sets of spots organized in mirror symmetry about the projection of the vertical nanotube axis. In addition, two intense spots are aligned perpendicular to the nanotube axis and labeled (0,0,4) in the usual (h,k,l) crystallographic notation.

The latter spots are most easily understood. They are produced by electron diffraction from the two sets of parallel quasiplanar graphene sheets whose projections are shown in Fig. 5(a): such planes, seen edge on, act as two parallel line gratings for the electron waves. The intensities scattered by the left and right gratings add up with negligible interferences. The spots belong to a series of equidistant $(0,0,2m)$ spots where the integer m is the diffraction order (the factor 2 arises from the double layer spacing periodicity of graphite in the $ABAB$ hexagonal stacking). The first-order (0,0,2) spots are buried in the (0,0,0) unscattered beam while the third-order (0,0,6) spots are unresolvably weak because the gratings have only three lines (as is well known from elementary diffraction theory, the diffracted intensities grow with the number of lines in the grating). And, indeed, all of the $(0,0,2m)$ spots up to $m=3$ are clearly seen in the micrographs of Fig. 6, which shows the diffraction image of a nanotube with many more layers (Amelinckx *et al.*, 1999a, 1999b).

Turning now to the circular sets of spots in Fig. 5(b) or Fig. 6, they represent the diffraction by the rest of the nanotube, namely, the two stacks of hemicylindrical honeycomb sheets, seen face on, upstream and downstream of the beam. To understand this and interpret further the details of the patterns, we need to consider the detailed arrangement of atoms expected in single- and multiple-wall nanotubes (Iijima, 1991).

B. Construction of a nanotube

The way to construct a single-wall nanotube from a flat graphene sheet is shown in Fig. 7(a). An atomic lattice point (L,M) is brought into coincidence with the lattice origin (0,0) by rolling up the graphene sheet and bonding its two lateral edges. The two integers L and M completely determine the nanotube, apart from its length and end caps, which are left unspecified. Three examples are shown in Figs. 7(b)–(d). One sees that achiral or chiral nanotubes can result from this construc-

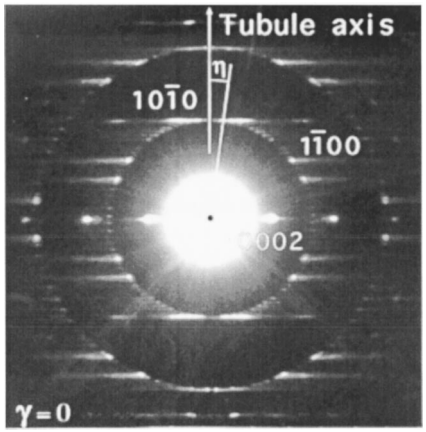

FIG. 6. Electron-diffraction micrograph of a multiwall nanotube (about 20 layers) perpendicular to the electron beam. The Bragg diffraction circles are produced by the cylindrical honeycomb lattices of each layer. A few pairs (perhaps four or five pairs) of hexagons of streaking spots can be counted on each diffraction circle (the outer circle is an enlarged version of the inner one turned by 30°). η is the chiral angle of the layers producing the prominent pair of spots marked $1\bar{1}00$ (an alternate notation for a hexagonal lattice node). The family of equidistant spots on the equator line, the first marked 0002, are produced by the double grating of the nanotube wall such as the one seen in projection in Fig. 5(a).

tion. Recall that, by definition, an achiral object is one which can be superposed to its mirror image whereas a chiral one cannot (like the left or right hand). Single-wall nanotubes of type (L,L) or $(L,0)$ are manifestly achiral; (L,L) types are called "armchair" or "perpendicular" nanotubes [they have a family of C-C bonds perpendicular to the tube axis, Fig. 7(b)], whereas $(L,0)$ types are called "zigzag" or "parallel" nanotubes [C-C bonds parallel to the axis, Fig. 7(c)]. All other nanotubes with $L \neq M \neq 0$ are chiral (conventionally right handed when $L > M$ or left handed otherwise). Chiral nanotubes can be characterized, in three equivalent ways, by a chiral angle α which is uniquely determined by the couple (L,M). Most often one takes α to be the angle between the nanotube diameter and the nearest zigzag line of atoms, as shown in Fig. 7(a). Armchair (L,L) and zigzag $(L,0)$ nanotubes have a rotation axis of order L and are periodic in the direction of the axis with period $d\sqrt{3}$ and $3d$, respectively, where $d = 0.14$ nm is the C-C bond length. Chiral nanotubes have a screw axis and a less obvious axial periodicity. This can be seen by inspection of the nanotube construction scheme of rolling up a flat graphene sheet [Fig. 7(a)].

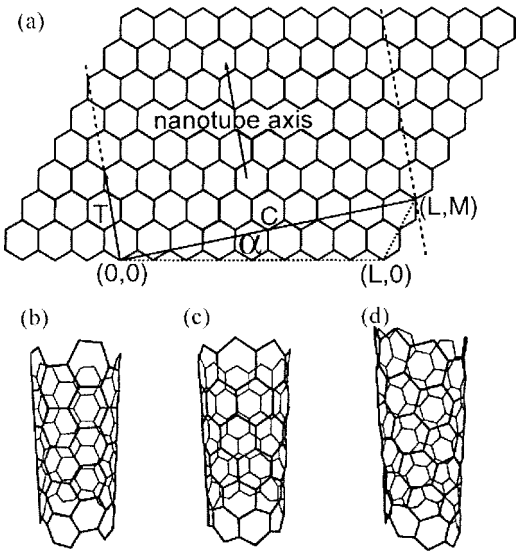

FIG. 7. Construction of a single-wall nanotube: (a) defining the two integers (L,M) which are necessary and sufficient to construct a single-wall nanotube by bringing the lattice point (L,M) in coincidence with the lattice origin (0,0). C is the nanotube circumference while T is its axial repeat period. α is the chiral angle; (b) achiral, armchair or perpendicular (5,5) single-wall nanotube; (c) achiral, zigzag or parallel (9,0) single-wall nanotube; (d) chiral (7,3) single-wall nanotube.

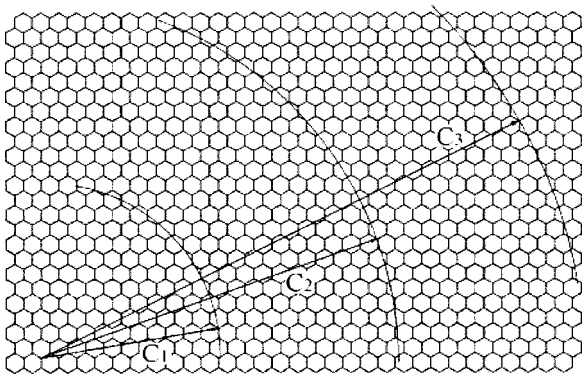

FIG. 8. Constructing, on a flat graphene sheet, the possible (L,M) indices of a nanotube comprising three layers of specified circumferences C_1, C_2, C_3. Note that for large-diameter nanotubes, several (L,M) lattice points are acceptable as they fall onto or very near the circumference.

The graphical construction of a multiwall nanotube follows from the previous method. One has to assemble several single-wall nanotubes coaxially by maintaining the canonical graphitic distance between the layers. An example of constructing a three-layer nanotube is illustrated in Fig. 8. Pairs of integers (L,M) are chosen such that the corresponding nanotube circumference increases by $0.34\,\text{nm} \times 2\pi$ from one layer to the next. A certain tolerance (of perhaps 0.01 nm) in the choice of nanotube radii is acceptable given the finite accuracy of size determination in experimental electron micrographs. From Fig. 8, it is then apparent that the precise (L,M) couples and hence the chiral angles of individual layers are rather ill defined by the radius criterion alone because a curve of given circumference (such as C_3) passes close to several nodes of the graphene lattice. Fortunately the electron diffraction pattern of a multiwall nanotube comprising but a few layers (such as the three-layer nanotube of Fig. 5) provides, as we shall see, a direct reading of the set of chiral angles present in the nanotube, independent of the set of radii.

In principle there could be as many different chiral angles as layers in a multiwall nanotube. In practice,

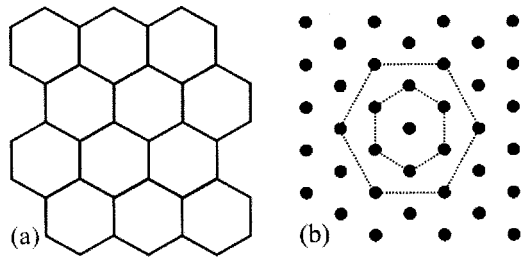

FIG. 9. Diffraction by a honeycomb lattice: (a) a flat lattice of trigonal bonds; (b) diffraction pattern (Fourier transform) of (a).

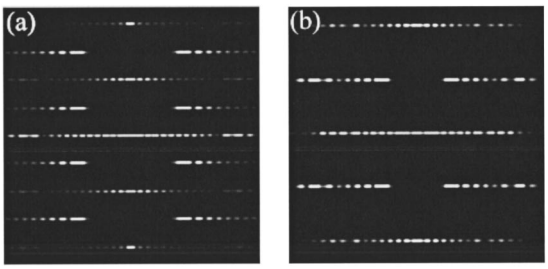

FIG. 10. Diffraction by achiral nanotubes: (a) Computer simulation of the (normal incidence) diffraction pattern of a (19,0) single-wall nanotube; (b) same for a (12,12) single-wall nanotube.

however, electron-diffraction observations indicate that, in nanotubes comprising many layers, the number of different chiral angles is often substantially less than the number of layers. For example, in the multiwall nanotube of Fig. 6, the layers must be arranged into groups having the same chirality because no more than four or five different chiral angles are counted from the number of spots on the Bragg circles (see below). This suggests that the growth process of the multiwall nanotube probably proceeds sequentially, inwardly or outwardly, i.e., each additional new layer would nucleate and grow locally onto the previous one by a process of partial epitaxy[1] causing some deviations of the interlayer distances from the equilibrium 0.34-nm value. Such a process would tend to maintain the chiral angle constant over several layers until the strain accumulated by the slightly wrong radii would force a change of chirality in the next layer or group of layers.

C. Diffraction by flat graphene

To understand better the diffraction by a nanotube, one should first recall the kind of two-dimensional diffraction pattern which is produced by a flat honeycomb lattice. This is shown in Figs. 9(a) and (b). The diffraction spots are on a triangular lattice, the reciprocal nodes of the triangular Bravais lattice underlying the honeycomb atomic lattice. The spots form hexagons which lie on discrete circles of increasing diameters around an arbitrary origin in reciprocal space. Two hexagons of successive orders are rotated by 30°. The first-order reciprocal hexagon is oriented parallel to the atomic honeycomb hexagons.

D. Diffraction by single-wall nanotubes

Observing the diffraction pattern of a single-wall nanotube is rather difficult. The spot pattern is quite weak due to the relatively small electron scattering power of carbon atoms and the small number of atoms in the electron path. This requires a long exposure time, which results in a tendency for the nanotube to be destroyed by the energetic electrons of the microscope (several hundreds of keV). For this reason, we will discuss here only computer-simulated patterns of single-wall nanotubes, which will then allow us to understand the real diffraction patterns of multiwall nanotubes, such as those of Figs. 5 and 6. The simulations are based on an exact kinematical diffraction theory for nanotubes developed recently (Lambin *et al.*, 1997; Qin *et al.*, 1994, 1997) whose explanation goes beyond the scope of the present paper. The examples chosen here for the computer simulations will also be simulated optically.

An achiral single-wall nanotube should produce hexagonal sets of diffraction "spots" similar to those of a flat graphene sheet and having the (projection of the) tube axis as symmetry axis. Indeed in an achiral single-wall nanotube, the two curved faces of graphene situated upstream and downstream of the electron beam project as identical honeycomb lattices distorted by the sheet curvature. This planar projection can serve to predict qualitatively the diffraction by the real three-dimensional nanotube. This is because, in electron-diffraction experiments using high-energy electrons on very small specimens, the appreciable elastically scattered intensities appear only at very small scattering angles for which the diffraction pattern of the real 3D object can be shown to be very close to that which would be produced by its planar 2D projection parallel to the electron beam (Lucas *et al.*, 1999).

Two simulated diffraction patterns are shown in Figs. 10(a) and (b) for (20,0) and (11,11) single-wall nanotubes seen at normal incidence. The curvature distortion introduces modifications of the hexagonal diffraction pattern of a flat sheet: the observed spots in Fig. 10 are not the sharply defined circular features of Fig. 9(b) but are diffuse, comma-shaped streaks. The streaks are sharp only in the direction of the nanotube axis (along which the nanotube periodicity is indeed the same as in the flat graphene sheet). But they are elongated perpendicular to the axis: they begin brightly from the nominal spot positions on the diffraction circles and fade away from the axis (the origin of the streaking will be explained below).

[1]Another interpretation is to assume that the multiwall nanotube is in fact made, at least in part, of several multiturn graphene scrolls rather than seamless cylinders, one scroll having a single conserved chirality at each turn. Distinguishing between the two interpretations via the electron diffraction patterns alone is impossible; see Amelinckx *et al.* (1999a, 1999b) and the discussion in Sec. II.A.

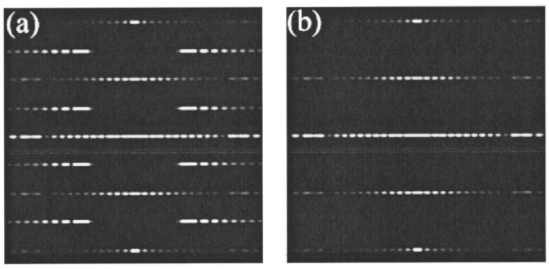

FIG. 11. Extinction of some layer lines by rotating the nanotube: (a) diffraction pattern of a (19,0) single-wall nanotube [same as Fig. 10(a)]. The nanotube is oriented around its axis in such a way that the projections of the back and front sides of the nanotube coincide; (b) same as (a) but with a $\pi/2L$ rotation of the nanotube such that the back and front projected lattices are shifted by half a lattice period. Compare to (a) and note the extinction of every other layer line.

The relative position of the projections of the upstream and downstream faces of the single-wall nanotube depends on the nanotube angular position around its axis: rotating the nanotube produces a periodic shift of period π/L of the 2D projections with respect to each other. Such a rotation can have a strong effect on the intensities of the diffracted streaks as a result of interferences between the waves scattered by the two faces. This is shown in Figs. 11(a) and (b) and will also be demonstrated by optical simulations.

A *chiral* single-wall nanotube produces two hexagonal sets of streaking spots rotated symmetrically with respect to the previous achiral set, as shown in the computer simulations of Figs. 12(a) and (b) for a (19,2) and a (12,10) single-wall nanotube. One hexagon is the result of diffraction by the upstream, hemicylindrical portion of the tube and the other by the downstream part. The rotation angle separating the two hexagons is twice the chiral angle α, which is therefore directly measurable from the diffraction pattern. The accuracy of this measurement is, however, somewhat limited by the difficulty in pinpointing the streak maximum.

We now provide a qualitative interpretation of the streaking phenomenon seen in the simulations as well as in the electron-diffraction patterns of Figs. 5 and 6. When the electron beam travels towards a nanotube, it sees the honeycomb lattice of the curved graphene sheet as having a well-defined and constant lattice spacing

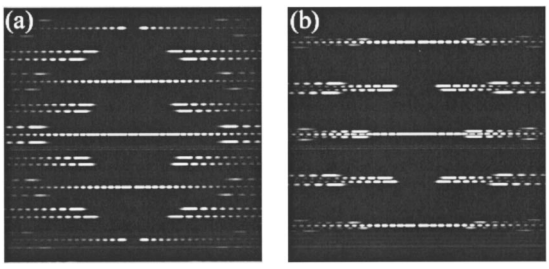

FIG. 12. Diffraction by chiral nanotubes: (a) diffraction pattern of a (19,2) single-wall nanotube; (b) diffraction pattern of a (12,10) single-wall nanotube.

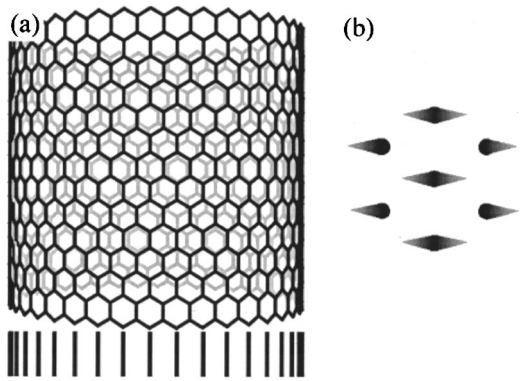

FIG. 13. The streaking of the diffraction spots: (a) perspective view of a nanotube showing the chirping of the apparent (projected) honeycomb lattice parameter perpendicular to the nanotube axis as one approaches the nanotube wall; (b) the quasicontinuous change of lattice parameter causes the streaking of the diffraction spots away from the nanotube axis.

along the nanotube axis. The diffraction will then give rise to spots which remain sharp in the direction along the nanotube axis, as already stated above. However, the electron waves see a shrinking lattice parameter along the nanotube circumference: towards the nanotube edges the hexagons are looked upon at an increasingly grazing angle, as illustrated in Fig. 13(a) for a (36,0) single-wall nanotube. Hence the diffraction spots should be elongated away from the axis [Fig. 13(b)], that is, towards larger diffraction angles since produced by apparently shorter lattice spacings. The intensity of each spot increases towards the axis and ends up at the nominal hexagonal position. The maximum intensity occurs there because the 90° angular orientation of the honeycomb lattice perpendicular to the beam represents an extremum of this orientation. According to the simplified view presented here, the streaking is the analog, in wave-vector space, of what is known as "chirping" in the frequency domain and is the reciprocal of the real-space apparent chirping of the lattice spacing around the nanotube circumference (Fig. 13). However, it should be noticed in Figs. 10–12 that the streak intensity does not vary continuously as predicted by this simple model but is modulated. The modulation is caused by the interference of the electron waves diffracted by the left and right sides of the nanotube, as in the fundamental Young two-slit diffraction experiment. The modulation period is a measure of the inverse of the nanotube diameter.

E. Diffraction by multiwall nanotubes

Now that the electron diffraction pattern of a single-wall nanotube is understood, it is straightforward to interpret that of a multiwall nanotube. The total diffracted electron amplitude for a multiwall nanotube should be the simple addition of the amplitudes scattered by its individual single-wall nanotubes. Apart from the $(0,0,2m)$ spots which do require the coherent addition of the diffraction amplitudes, the intensity of the other features is approximately the sum of the individual in-

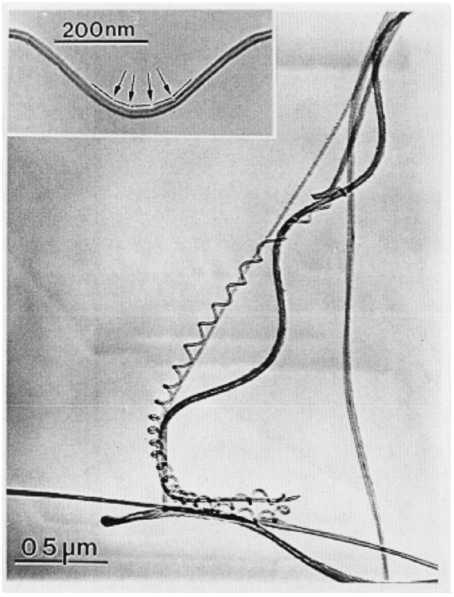

FIG. 14. Low resolution electron micrograph of a multiwall nanotube sample showing several coiled nanotubes with various diameters and periods. The higher-resolution image of the inset hints at a polygonized structure of the coil.

tensities: on each diffraction circle, there should be one pair of spot hexagons contributed by all nanotubes sharing the same chirality. If there were no correlation between the chiralities of successive layers, there would be twice as many hexagons as layers. Then the overall pattern of a multiwall nanotube with many layers would resemble that of a graphite powder pattern, i.e., a set of quasicontinuous circles similar to the Bragg circles of a polycrystalline material. But in practice, even nanotubes having several dozen layers (such as the one producing the pattern of Fig. 6) still exhibit countable, discrete sets of hexagon pairs. As explained before, this reflects a quasiepitaxial growth mechanism and eventually allows one to enumerate the different chiral angles contained in the multiwall nanotube (Amelinckx *et al.*, 1999a, 1999b).

F. Coiled nanotubes

A method of nanotube synthesis, based on cracking hydrocarbon molecules on the surface of a metal catalyst (Bernaerts *et al.*, 1995), frequently produces multiwall nanotubes curiously shaped as regular coils resembling telephone cords. One electron microscopy picture showing several such coils is given in Fig. 14. Figure 15(b) is the diffraction pattern of a selected area covering about one period of a coiled helix [Fig. 15(a)]. The main features of the pattern, namely, the successive diffraction circles and the strong circular arcs, are easily correlated with those of a straight multiwall nanotube. As one progresses along the coil the orientation of the nanotube axis describes a cone and therefore the angular orientation of the honeycomb lattices with respect to the electron beam axis oscillates. This causes the hexagonal set of diffraction spots of the multiwall nanotube

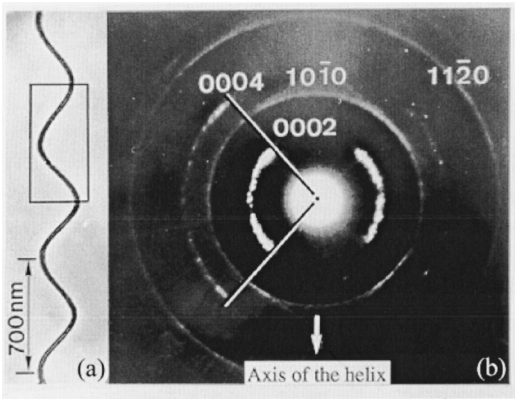

FIG. 15. Electron micrograph image of a coiled nanotube and its diffraction pattern: (a) high-resolution electron micrograph of a coiled nanotube projecting as a sine wave; (b) electron diffraction of (a) obtained by illuminating an aperture covering one single nanotube period [rectangle in (a)]. The (0002) spots form a discrete spotty arc.

to rock around its center and to produce a quasicontinuous Bragg diffraction circle quite similar to that of a graphite powder pattern. On the other hand, the discrete $(0,0,2m)$ spots of the equatorial layer line of the multiwall nanotube are made to describe circular arcs whose amplitude is equal to the cone opening angle. Note carefully, however, that the arcs are spotty, as if only certain discrete orientations of the nanotubes were realized. Electron microscopy pictures at high resolution have indeed confirmed that the coiled multiwall nanotube are in fact made of a regular succession of about 12 straight cylindrical pieces somehow connected to each other at sharp bends of about 30° (Bernaerts *et al.*, 1995).

The optical simulations which follow will attempt to reproduce these spectacular features.

III. OPTICAL SIMULATIONS

The optical simulation method (also called the optical transform method, because it produces Fourier transforms) has been introduced by one of the founding fathers of diffraction, W. L. Bragg (1939, 1944) himself. Short wavelength radiations (x rays, electrons, neutrons, etc.) are replaced by a monochromatic beam of visible light and the diffracting atomic objects (crystals, biomolecules, etc.) are replaced by suitable optical gratings on a slide. With lasers as light sources, the diffraction patterns are clearly visible on a white screen a few meters away without the need to use any additional, post-specimen optics.

Consider the electron case. When simulating the diffraction of electrons from a nanoscale molecular structure such as a nanotube (diameter of order 1 nm), the de Broglie wavelength of electrons typically used (about 0.002 nm for 300 keV) is scaled up to the red light wavelength of a He-Ne laser or a laser pointer (about 650 nm). The corresponding upscaling of the size of the nanotube brings it in the comfortable submillimeter

range easily reached by photographic reduction of a macroscopic model of the nanotube. A hand or computer drawing of a nanotube on a standard size sheet of paper is first realized. The photoreduction then produces the desired diffraction grating on a standard slide. Note that the actual, absolute size of the model in the submillimeter range is not crucial. Indeed, the light of a laser remains spatially coherent over its beam width (i.e., several mm), so that decreasing the size of the diffraction motif would simply increase the size of the diffraction pattern proportionately, an effect which can be achieved in a simpler manner by moving the projection screen further away.

The scattering mechanism (and hence the scattered intensities) of electrons by a nanotube may be quite different from that of visible light by the film model, but the geometrical arrangement of the diffraction patterns should be very similar (Lucas *et al.*, 1999), which is all that is required of the present qualitative simulations.

For a faithful simulation of a selected area electron diffraction of a nanotube, one single diffracting nanotube model should in principle be used. This is possible, but in practice the intensities obtained from one single motif are too weak to be useful for easy observation. This is why one preferably makes multiple, parallel, well separated copies of the nanotube model on the same slide. The intensities are thereby enhanced about proportionately to the number of copies intercepted by the optical beam. In order to eliminate the periodicity in the diffraction pattern which would be created by a spatially regular repeat of the copies, it is recommended to introduce a degree of randomness in their interdistance.

There are two ways to observe the diffraction patterns. The direct or collective method is convenient and requires just one diffraction slide: one passes the beam of a laser pointer through the slide and projects the pattern onto a white screen a few meters away. The individual method requires multiple copies of the slide: one provides a slide to each viewer who looks through the slide held near the eye towards a distant point source of light. The diffraction pattern is then clearly visible at the level of the slide itself. The point source may be a bare laser spot reflected on a white screen. But interestingly, a simple white flash lamp will also work with this individual method, provided the source is distant enough. Using a white flash lamp eliminates the somewhat hazardous use of lasers and has the additional merit of showing dispersion effects in the form of colored diffraction fringes.

A "diffraction laboratory" on a slide has been prepared. It contains nine distinct panels, each of which is large enough to accommodate the full laser beam width. Figures 16(a)–(i) show the nine diffraction motifs of the panels. All the optical simulations presented in this paper are made with this typical single slide. Needless to say, many variants of the slide can be prepared to obtain optical transforms of other two-dimensional atomic patterns (Lisensky *et al.*, 1991) or other single and multiple-wall nanotubes.

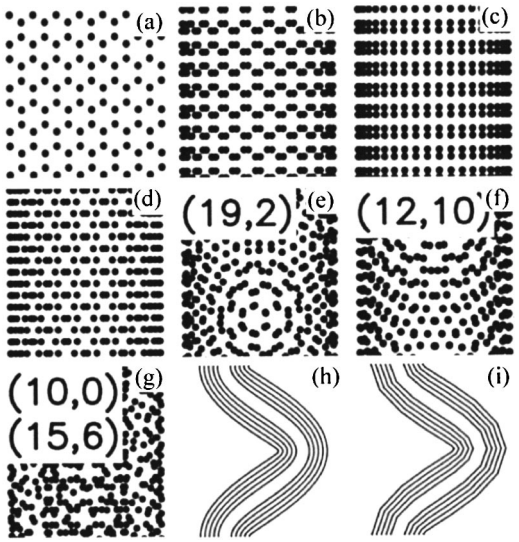

FIG. 16. Diffraction motifs to simulate optically the electron diffraction by various nanotubes. The diffraction motifs (a)–(i) are all on one single standard slide.

Figure 16(a) is a simple honeycomb lattice of dots whose 2D Fourier transform is the hexagonal lattice of point nodes shown in Fig. 17(a). The latter is a photograph of the actual laser pattern produced with a good, class IIIa laser pointer and can be compared with the computer picture of Fig. 9(b).

The nanotube motif shown in Fig. 16(b) consists in the planar projection of a (20,0) single-wall nanotube perpendicular to its axis. A choice had to be made to represent the atoms in this and the following motifs, in such a way as to represent somehow the atomic scattering factor of the unit cell. Here the carbon atoms have been represented as fat, black-on-white circular dots with

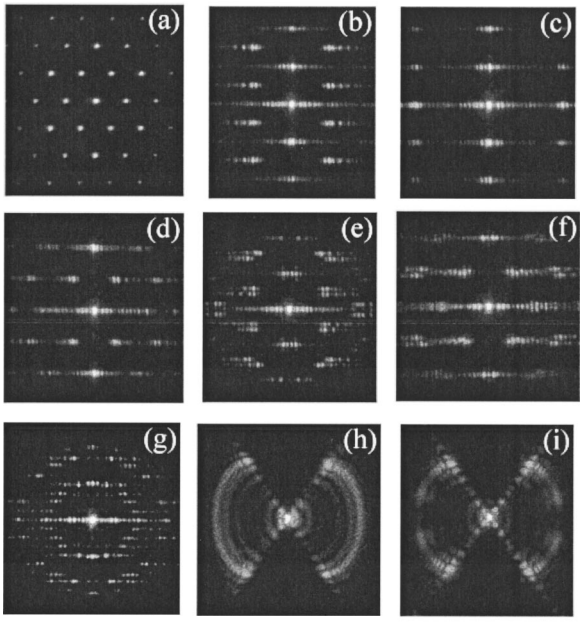

FIG. 17. Photos of the nine optical diffraction patterns produced by Figs. 16(a)–(i) using a red laser pointer.

sharp edges centered on the nuclear positions. This generally works well to simulate high-energy electron diffraction from any material, in view of the nature of the electron scattering mechanism (i.e., by the isotropic screened Coulomb potential of the atomic nuclei). Although we are concerned primarily with the geometry of the diffraction pattern rather than with the absolute spot intensities, more faithful atomic models could be tried such as smooth dots with a gray-scale profile mimicking the Fourier transform of the atomic scattering factor. However, this sophistication might prove counterproductive (we have not tried it) by decreasing drastically the optical pattern intensity to values comparable to the electron-diffraction patterns themselves. We believe that the efficiency of the optical simulation relies on the large scattering power associated with the sharp edges of the black-and-white dots. Simulation of atoms of different chemical species could still be done optically simply by varying the size of the dots.

The optical transform pattern of Fig. 17(b) compares quite closely with the computer simulation in Fig. 10(a). The layer lines, the hexagonal sets of spots on successive Bragg circles, the streaking of the spots perpendicular to the nanotube axis are all correctly simulated. In effect what the computer does in a few milliseconds, light does at the "lightning speed" of 10^{-14} sec (Bragg, 1939). The intensity modulation of the equatorial layer line and the streak modulation are also present in the optical transform. However, the modulations do not faithfully represent those of a single motif because of the residual interferences between the light diffracted by the repeated nanotube motifs within the light beam.

The pattern of Fig. 17(c) produced by the motif of Fig. 16(c) illustrates the sensitivity of the diffraction pattern of a single-wall nanotube on its rotational orientation around its axis, as already seen in the computer simulation of Fig. 11(b): if the upstream and downstream part of the single-wall nanotube are shifted by $\pi/2L$, the axial translation periodicity of the nanotube projection is divided by 2 ($3d/2$ instead of $3d$). As a consequence, the diffraction spots in the reciprocal space are two times more spaced along the vertical nanotube axis.

A series of three other single-wall nanotube motifs and the corresponding optical transforms are shown in Figs. 16(d)–(f) and 17(d)–(f). For chiral single-wall nanotubes, the characteristic doubling of each diffracted hexagon is clearly revealed, allowing the measurement of the chiral angle from the diffraction pattern. The optical transforms should be compared to the computer simulations of Figs. 10(b), 12(a), and 12(b).

Figure 16(g) is for a multiwall nanotube made of one armchair (10,0) nanotube and one chiral (15,6) nanotube separated by 0.34 nm. In Fig. 17(g), three hexagonal sets of streaking spots are seen, one for the achiral and two for the chiral nanotube. In addition, the equatorial line now shows a strong modulation of the intensity corresponding to the embryonic $(0,0,2m)$ spots created by the 0.34-nm repeat.

Finally, Figs. 16(h) and 16(i) are two representations of a coiled, five-layer multiwall nanotube. Only the projections of the lateral walls of the nanotubes onto a plane containing the coil axis are represented as continuous lines, each layer being assumed to be a continuous, hollow helical tube. Here a single, unrepeated motif has sufficient scattering power to produce a visible diffraction pattern. In Fig. 16(h) the tube axis follows a smooth helix, while in Fig. 16(i) the layers (and their axis) are polygonized into 12 pieces of straight circular cylinders joined to each other at sharp bends of about 30°. The optical transforms in Figs. 17(h) and (i) consist of a series of diffraction arcs which represent the loci of the $(0,0,2m)$ spots on the "equatorial" layer line perpendicular to the local nanotube axis. Since the direction of the latter changes periodically and describes a cone when moving along the helix, the layer line sweeps an angle whose opening bears a simple relationship to the amplitude of the helix as compared to its period. The distribution of intensity along the arcs is continuous in Fig. 17(h) and discretized in Fig. 17(i), consistent with the continuous or polygonized nature of the motifs. Finally the intensities are maximum at the arc extremities reflecting the extremum nature of the nanotube orientation for these directions. All these features of the optical transforms are quite realistic representation of the actual features of the electron diffraction patterns in Fig. 15(b).

IV. SUMMARY

This paper has used the method of "optical transform" to simulate the formation of the diffraction patterns produced by single carbon nanotubes such as observed by high-resolution electron microscopy and electron diffraction or calculated by theoretical simulations. The aim was to arrive at a qualitative understanding of all the features of the observed or computer simulated patterns without having recourse to either the somewhat involved theory of kinematic wave scattering by a nanotube (Lambin *et al.*, 1997; Qin *et al.*, 1994) or the rather intricate geometrical reasoning in the reciprocal space of the nanotube (Amelinckx *et al.*, 1999a, 1999b).

Easily manufactured, two-dimensional optical masks on a slide representing scaled up planar projections of the atomic distribution of nanotubes served as diffraction gratings for the visible light of a coherent source (such as a laser pointer). The distances between "atomic" features in the optical gratings are in the convenient submillimeter range and can be viewed with an ordinary slide projector or a magnifier. No special "optics" is required to obtain large diffraction patterns, which are clearly visible even in broad daylight and which can be directly compared to the experimental or computer-simulated electron micrographs.

In the electron microscope, post-specimen magnification is used not only for building a high-resolution image of the specimen itself but also for observing the diffraction pattern which otherwise would be too small (or require a prohibitively long, post-specimen vacuum chamber) on account of the very small scattering angles. In

the optical transform simulations, no post-specimen optics is necessary by virtue of the fact that strong laser intensities are maintained over many tens of meters.

In view of the ease with which optical masks can be prepared by computer, the present optical transform method could be of further use in this field in order to test current structural ideas on the atomic arrangements in nanotube junctions (Léonard *et al.*, 2000; Meunier *et al.*, 1998), nanotube ropes and lattices (Henrard *et al.*, 1999), polygonized nanotubes (Moreau *et al.*, 2001), etc., as well as in heterostructures such as in BN (Loiseau *et al.*, 1996) and WS_2 (Tenne *et al.*, 1992) nanotubes or nanotubes with a large population of defects.

ACKNOWLEDGMENTS

We are grateful for the support of the following agencies: the Belgian National Science Foundation, the Fund for Industrial and Agricultural Research FRIA, the Ministry of Sciences, the European Commission TMR program, and the Walloon Government. We thank Professor S. Iijima for allowing us to reproduce Fig. 5 and Professor S. Amelinckx for Figs. 6, 14, and 15 and for a fruitful collaboration.

REFERENCES

Amelinckx, S., A. A. Lucas, and Ph. Lambin, 1999a, in *The Science and Technology of Carbon Nanotubes*, edited by K. Tanaka, T. Yamabe, and K. Fukui (Elsevier Science, Amsterdam), p. 14.

Amelinckx, S., A. A. Lucas, and Ph. Lambin, 1999b, "Electron diffraction and microscopy of nanotubes," Rep. Prog. Phys. **62**, 1.

Bernaerts, D., X. B. Zhang, X. F. Zhang, S. Amelinckx, G. Van Tendeloo, J. Van Landuyt, V. Yvanov, and J. B'Nagy, 1995, "Electron microscopy study of coiled carbon nanotubes," Philos. Mag. A **71**, 605.

Bragg, W. L., 1939, "A new kind of "x-ray microscope," " Nature (London) **143**, 678.

Bragg, W. L., 1944, "Lightning calculations with light," Nature (London) **154**, 69.

Curl, R. F., and R. E. Smalley, 1991, "Fullerenes: The third form of pure carbon," Sci. Am. **264**, 54.

Dekker, C., 1999, "Carbon nanotubes as molecular quantum wires," Phys. Today **52** (5), 22.

Ebbesen, T. W., 1994, "Carbon nanotubes," Annu. Rev. Mater. Sci. **24**, 235.

Ebbesen, T. W., 1996, "Carbon nanotubes," Phys. Today **49** (6), 26.

Ebbesen, T. W., and P. M. Ajayan, 1992, "Large-scale synthesis of carbon nanotubes," Nature (London) **358**, 220.

Henrard, L., E. Hernández, P. Bernier, and A. Rubio, 1999, "van der Waals interaction in nanotube bundles: Consequences on vibrational modes," Phys. Rev. B **60**, R8521.

Huffman, D. R., 1991, "Solid C60," Phys. Today **44**, 22.

Iijima, S., 1991, "Helical microtubules of graphitic carbon," Nature (London) **354**, 56.

Iijima, S., 1994, "Carbon nanotubes," MRS Bull. **19**, 43.

Krätschmer, W., L. D. Lamb, K. Fostiropoulos, and D. R. Huffman, 1990, "Solid C60: A new form of carbon," Nature (London) **347**, 354.

Kroto, H. W., J. R. Heath, S. C. O'Brien, R. F. Curl, and R. E. Smalley, 1985, "C60: Buckminsterfullerene," Nature (London) **318**, 162.

Lambin, Ph., and A. A. Lucas, 1997, "Quantitative theory of diffraction by carbon nanotubes," Phys. Rev. B **56**, 3571.

Léonard, F., and J. Tersoff, 2000, "Negative differential resistance in nanotube devices," Phys. Rev. Lett. **85**, 4767.

Lisensky, G. C., T. F. Kelly, D. R. Neu, and A. B. Ellis, 1991, "The optical transform. Simulating diffraction experiments in introductory courses," J. Chem. Educ. **68**, 91.

Loiseau, A., F. Willaime, N. Demoncy, G. Hug, and H. Pascard, 1996, "Boron nitride nanotubes with reduced numbers of layers synthesized by arc discharge," Phys. Rev. Lett. **76**, 4737.

Lucas, A. A., Ph. Lambin, R. Mairesse, and M. Mathot, 1999, "Revealing the backbone structure of B-DNA from laser optical simulations of its x-ray diffraction diagram," J. Chem. Educ. **76**, 378.

Meunier, V., L. Henrard, and Ph. Lambin, 1998, "Energetics of bent carbon nanotubes," Phys. Rev. B **57**, 2586.

Moreau, F., Ph. Lambin, A. A. Lucas, J. C. Dore, *et al.*, 2001, "Neutron diffraction analysis of a nanotube powder produced by arc discharge," Phys. Rev. B (in press).

Qin, L. C., 1994, "Electron diffraction from cylindrical nanotubes," J. Mater. Res. **9**, 2450.

Qin, L. C., T. Ichihashi, and S. Iijima, 1997, "On the measurement of helicity of carbon nanotubes," Ultramicroscopy **67**, 181.

Tanaka, K., T. Yamabe, and K. Fukui, editors, 1999, in *The Science and Technology of Carbon Nanotubes* (Elsevier Science, Amsterdam).

Tenne, R., L. Margulis, M. Genut, and G. Hodes, 1992, "Polyhedral and cylindrical structures of tungsten disulfide," Nature (London) **360**, 444.

Zhen, Y., H. Ch. Postma, L. Balents, and C. Dekker, 1999, "Carbon nanotube intramolecular junctions," Nature (London) **402**, 273.